


Non-Hermitian complementary acoustic metamaterials for lossy barriers

Cite as: Appl. Phys. Lett. **115**, 051903 (2019); <https://doi.org/10.1063/1.5110501>
Submitted: 17 May 2019 . Accepted: 11 July 2019 . Published Online: 31 July 2019

Steven R. Craig, Phoebe J. Welch, and Chengzhi Shi 



View Online



Export Citation



CrossMark

Applied Physics Letters

Mid-IR and THz frequency combs
special collection

[Read Now!](#)



Non-Hermitian complementary acoustic metamaterials for lossy barriers

Cite as: Appl. Phys. Lett. **115**, 051903 (2019); doi: [10.1063/1.5110501](https://doi.org/10.1063/1.5110501)

Submitted: 17 May 2019 · Accepted: 11 July 2019 ·

Published Online: 31 July 2019



View Online



Export Citation



CrossMark

Steven R. Craig,¹ Phoebe J. Welch,¹ and Chengzhi Shi^{1,2,a)} 

AFFILIATIONS

¹Meta Acoustic Lab, George W. Woodruff School of Mechanical Engineering, Georgia Institute of Technology, Atlanta, Georgia 30332, USA

²Parker H. Petit Institute for Bioengineering and Bioscience, Georgia Institute of Technology, Atlanta, Georgia 30332, USA

^{a)} Author to whom correspondence should be addressed: chengzhi.shi@me.gatech.edu

ABSTRACT

Complementary materials are designed for the suppression of strongly mismatched potential barriers to enhance wave transmission and reduce wavefront distortion through the barriers. In acoustics, complementary materials enable noninvasive brain imaging and the treatment of neural disorders by overcoming the high impedance mismatch layer that prevents ultrasound transmission. However, the porous skull layer possesses intrinsic loss that prohibits the effective use of complementary metamaterials alone. Here, we propose to apply a non-Hermitian complementary metamaterial (NHCMM) to counteract the impedance mismatch and energy attenuation effect of the skull to achieve high acoustic transmission at high frequencies. Our numerical study shows a near perfect, unidirectional transmission through the skull when the NHCMM is applied while preserving the imaging information and enhancing the acoustic energy at the focal point needed for focused ultrasound used for noninvasive therapies. The proposed acoustic NHCMM lays the foundation for noninvasive ultrasonic brain imaging through an intact skull by stimulating *in-vivo* deep brain circuitry research and treatments for neural disorders such as brain tumors and strokes.

Published under license by AIP Publishing. <https://doi.org/10.1063/1.5110501>

Acoustic waves are widely used in biomedical applications because of their biocompatibility and penetration depth through tissue.¹ In particular, high frequency ultrasound has been applied safely for imaging and medical diagnosis for decades.² Recently, the concentrated energy at the focal point of focused ultrasound was exploited in the development of noninvasive treatments for different diseases, including lithotripsy for kidney stones,³ ablation and histotripsy for tumors and thrombosis,^{4,5} thalamotomy for tremors,⁶ and drug delivery through the blood-brain barrier.⁷ Even with these significant impacts on biomedical imaging and therapies, ultrasound has not been applied for noninvasive brain imaging.

The presence of the skull inhibits noninvasive ultrasonic brain imaging due to a large impedance mismatch resulting in a strong reflection at the boundary of these two biomaterials.⁸ One approach for extraordinary acoustic transmission takes the advantage of the development of transformation acoustics⁹ and metamaterials¹⁰ to design an anisotropic complementary acoustic metamaterial (CMM) with negative material parameters that cancel out impedance mismatch effects.¹¹ While this is effective in enhancing the transmission through an energy conservative barrier, the intrinsic loss induced by the highly porous skull makes this method impractical.⁸ This loss is characterized by the imaginary parts of the material parameters and

significantly affects the total acoustic impedance. In addition, the intrinsic loss dampens a significant amount of acoustic energy that results in low wave transmission through the barrier that is infeasible for use in ultrasonic brain imaging.

In this work, we propose to apply a non-Hermitian complementary acoustic metamaterial (NHCMM) to counteract the strong impedance mismatch and intrinsic loss of the skull simultaneously for the realization of noninvasive ultrasonic brain imaging through an intact skull [Fig. 1(a)]. We aim to obtain the desired values of the NHCMM material parameters that enable near perfect transmission and wavefront restoration when high frequency ultrasound propagates through the combined layers of NHCMM and skull. To achieve this objective, we set up a simplified model consisting of the NHCMM and skull layers adjacent to each other [Fig. 1(b)]. The top part of the patient's head is assumed to be submerged in water; therefore, the background medium outside the human body is modeled as water as well as the brain due to its similar mechanical properties. In addition, only the longitudinal waves supported by water are considered first in this work. However, the effect of the shear wave propagation in the skull is investigated in the [supplementary material](#). By applying continuity boundary conditions at the each of the boundaries in Fig. 1(b), we observed that a solution given by $\rho_1 = -\rho_2$ and $c_1 = -c_2$ gives a

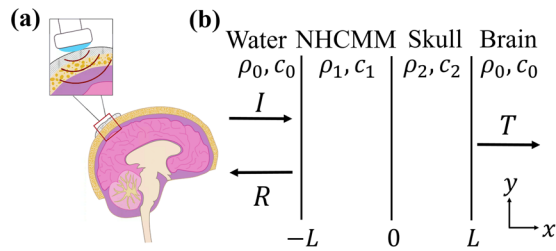


FIG. 1. NHCMM for noninvasive ultrasonic brain imaging. (a) Schematics of the application of NHCMM for ultrasonic brain imaging through an intact skull. (b) Simplified model of acoustic wave propagation through the combined NHCMM and skull layer with an incident wave outside of the top part of the patient’s head submerged in water. The acoustic properties of the brain are similar to those of water and are simulated as water.

total transmission ($T = 1$) and no reflection ($R = 0$). Variables ρ and c are the density and sound speed of longitudinal waves, and the subscripts 1 and 2 denote the NHCMM and skull, respectively. We note that ρ_2 and c_2 are complex-valued because of the intrinsic loss properties of the skull. Therefore, ρ_1 and c_1 are the direct opposite complex-valued material parameters of skull.

Physically, the opposite density and sound speed result in an identical acoustic impedance and an opposite refractive index of the NHCMM when compared with the skull. These material parameters suppress the impedance mismatch of the barrier,¹¹ while the opposite imaginary parts indicate that the NHCMM contains active gain materials that compensate the wave attenuation through the lossy skull

layer. The negative real parts of the NHCMM material parameters can be realized by resonating structures,^{12–15} while the imaginary parts are contributed by active gain elements, achievable by adding piezoelectric materials connected with amplification circuits used in the realization of parity-time (PT) symmetric acoustics,^{16,17} nonreciprocal propagation,¹⁸ and time reversal signal processing.¹⁹ Designing the circuit parameters to realize double negative complex material parameters operating in the desired frequency range is discussed further in the [supplementary material](#). While total transmission can be realized at the exceptional points of PT symmetric acoustics where active gain units were used,¹⁶ the physics of NHCMM and PT symmetric acoustics are completely different. PT symmetry requires the material parameters to satisfy $\rho_1 = \rho_2^*$ and $c_1 = c_2^*$,^{20–23} where the superscript * denotes the complex conjugate of the corresponding parameter, which does not hold for NHCMM. In physics, the total transmission and zero reflection are true for waves incident from both sides of the bilayer structure, making the whole system energy conservative.

Because the goal of this work focuses on obtaining the material parameters of the NHCMM for noninvasive ultrasonic brain imaging where high frequency acoustic waves are used, we conducted our calculations at 1.5 MHz. At this frequency, the measured effective density and sound speed of longitudinal acoustic waves are 1900 kg/m^3 and 2835 m/s with an acoustic attenuation of 25 dB through a 4 mm thick human skull sample.⁸ These acoustic properties are closely equivalent to complex-valued material parameters $\rho_2 = (1900 + 50i) \text{ kg/m}^3$ and $c_2 = (2835 + 80i) \text{ m/s}$ in numerical calculations. These values are obtained based on the loss characterization and parameter retrieval used in Refs. 18 and 24 where i is the imaginary unit. These complex-valued parameters are

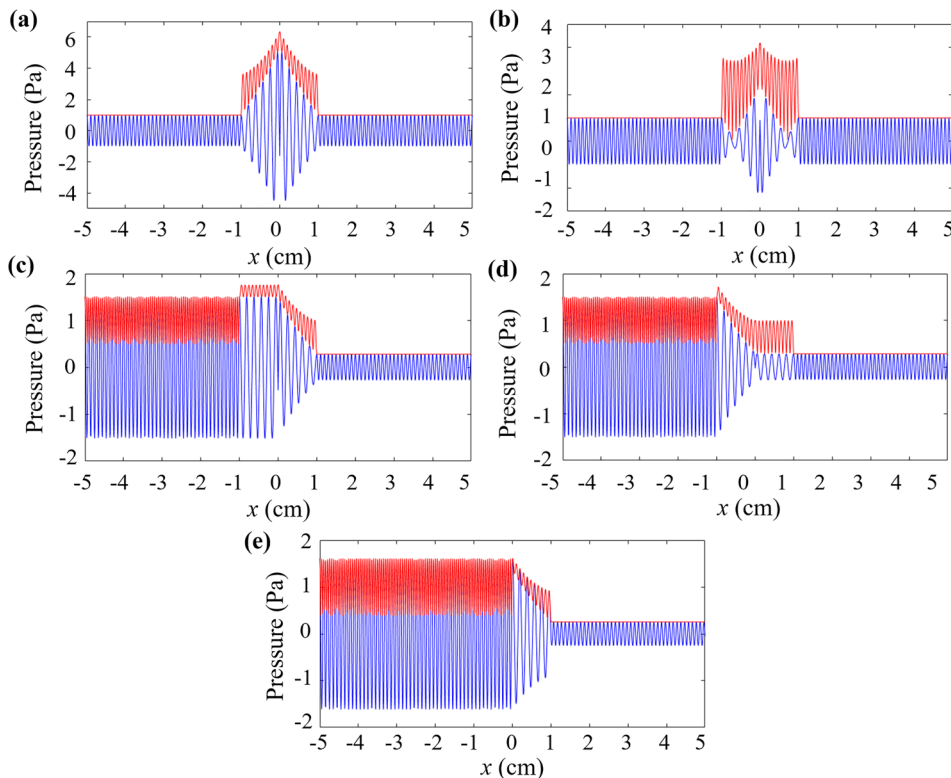


FIG. 2. Acoustic wave propagation through the skull when compensated by (a) and (b) NHCMM and (c) and (d) CMM. The skull thickness is between 0 and 1 cm, and the complementary layer is in between -1 and 0 cm for (a) and (c). The skull is in between -1 and 0 cm and the complementary layer is in between 0 and 1 cm for (b) and (d). (e) Acoustic wave propagation through the skull layer. For all cases, the red curve represents the acoustic amplitude, and the blue curve represents the acoustic field.

therefore used in our studies. From our analytical derivation listed above, the density and sound speed of the NHCMM are chosen to be $\rho_1 = -0.9999(1900 + 50i)$ kg/m³ and $c_1 = -0.9999(2835 + 80i)$ m/s to avoid singularity in the calculations. The density and sound speed of water and brain ($\rho_0 = 1000$ kg/m³ and $c_0 = 1500$ m/s) are used in our numerical calculations. The averaged thickness of human skull is $L = 1$ cm, which is used in this work. All numerical simulations are performed in COMSOL Multiphysics 5.3.

To analyze the transmission and reflection properties of the combined NHCMM and skull layer, we calculate an acoustic plane wave propagating through the bilayer structure from both incident sides [Figs. 2(a) and 2(b)]. The origin of the coordinate is set at the boundary between the NHCMM and skull, which are both 1 cm thick. For both cases, the transmission is 100% with no reflection, demonstrating the suppression of the loss skull barrier induced by the NHCMM. The sound speeds through the NHCMM and skull are of equal magnitude but opposite sign, resulting in an effective zero refractive index and hence no phase accumulation through the structure.^{25,26} The interference patterns in the bilayer indicate multiple reflections in between the boundaries. Thus, the energy damped by the lossy skull barrier is balanced by the gain of the NHCMM. For both incident cases, the highest acoustic amplitude occurs at the boundary between the NHCMM and skull. For the steady state, the peak acoustic amplitude reaches its highest value when the wave is incident from the water side due to the gain NHCMM amplifying the signal to a higher energy level before being damped by the lossy skull layer. In the opposite case, the wave is damped to a lower energy level in the skull layer before entering the gain medium incident from the brain side. Therefore, the energy needed to compensate the skull loss from the active gain element of the NHCMM is smaller when the wave is scattered back from the brain.

For comparison, the acoustic transmission and reflection from the skull compensated by a CMM are also calculated [Figs. 2(c) and 2(d)] with the transmitted acoustic energy reducing to 35% of the incident (12% in terms of energy), and a strong reflection is observed for incidence from either side. It is evident that the real part of the skull impedance is affected by the imaginary parts of the material parameters. The mismatched impedance induces an acoustic reflection boundary, and acoustic energy loss makes the CMM ineffective and insignificantly beneficial compared to the energy transmission direction through the skull [Fig. 2(e)].

The ultrasonic imaging performance is characterized by calculating the scattered acoustic field from a brain tumor through the skull complemented by the NHCMM [Fig. 3(a)]. The brain tumor is modeled by a circle with a 2-cm diameter located 2 cm away from the inner boundary of the skull. The density and sound speed of the brain tumor are set to be $\rho_t = 1500$ kg/m³ and $c_t = 2000$ m/s. For comparison, the scattered field from the same brain tumor without transmitting through the bilayer structure is calculated [Fig. 3(b)]. In this case, the field we look at is 2 cm closer to the tumor than the case where the skull is compensated by the NHCMM due to the lack of phase accumulation across the bilayer [Figs. 2(a) and 2(b)]. In both cases, the shadow lines of the brain tumor are observed in the reflected pressure amplitude fields. The pressure amplitude of the reflected wave along a line 2 cm away from the outer boundary of the NHCMM for both cases is plotted. The shadows are located at $y = \pm 1.8$ cm for both cases, indicating the existence of the circular brain tumor. These shadows demonstrate the effectiveness of the NHCMM. On the other

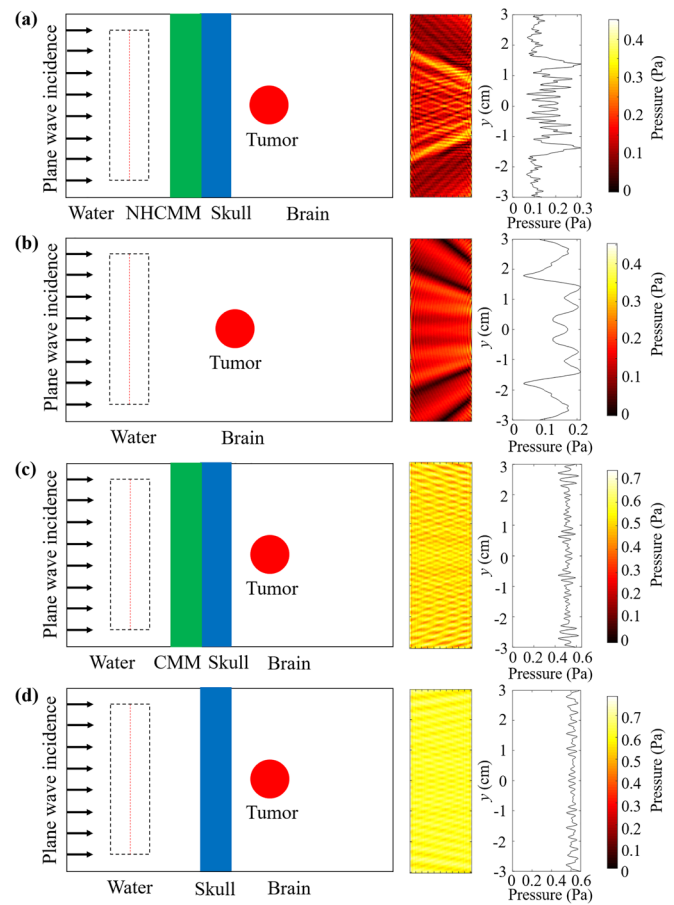


FIG. 3. Ultrasonic imaging of a brain tumor. (a) Imaging through the skull complemented by the NHCMM. (b) Direct imaging without the skull. (c) Imaging through the skull complemented by the CMM. (d) Imaging directly through skull. For (a) and (c), the amplitude of the reflected wave in the dashed rectangle (2 cm by 6 cm) with the right boundary 1 cm away from the outer boundary of the bilayer is shown. For (b), the brain tumor is shifted 2 cm to the left compared with the other cases. For (d), the right boundary of the dashed space is 2 cm away from the outer boundary of the skull. The reflected pressure amplitudes along the red line at the middle of the dashed space for all cases are plotted.

hand, when the real-part based CMM is used, most of the acoustic energy is reflected back from the bilayer and no shadow of the brain tumor is found [Fig. 3(c)], similar to directly imaging through the lossy skull layer [Fig. 3(d)]. Thus, the brain tumor cannot be detected by ultrasound through the skull complemented by the CMM.

Another widely used type of acoustic wave in biomedical applications like neuron stimulations, ablation, thalamotomy, and drug delivery³⁻⁷ is focused ultrasound. The propagation of waves generated by a curved focused ultrasound transducer through the skull complemented by the NHCMM compared with the focused wave without the skull is also calculated [Figs. 4(a) and 4(b)]. The two cases have a similar focusing effect with almost the same amount of energy concentrated at the focal point. When the skull is complemented by the CMM, the acoustic energy has the same focal point, but at a much lower energy level [Fig. 4(c)]. This is because the refractive index of a

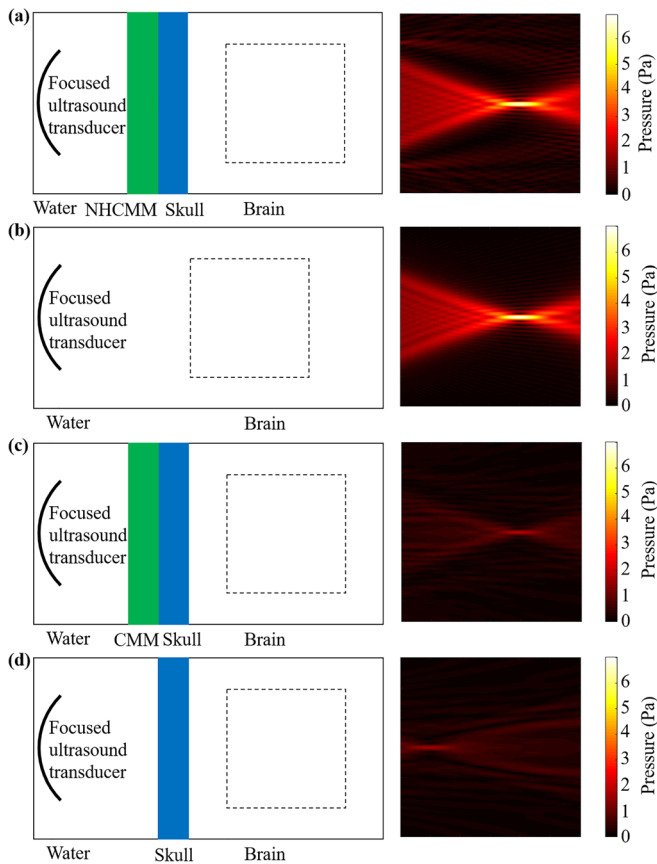


FIG. 4. Focused ultrasound generated by a curved transducer. (a) Focusing through the skull complemented by the NHCMM. (b) Focusing without the skull. (c) Focusing through the skull complemented by the CMM. (d) Focusing directly through the skull. The pressure amplitude in the square (6 cm by 6 cm) is shown. The left boundary of the square is 2 cm away from the inner boundary of the skull for (a), (c), and (d). The square is shifted 2 cm to the left for (b) compared with the other cases.

medium is determined by the real part of the sound speed. With the same real part of the sound speed, the refractive index of the CMM is identical to that of the NHCMM, resulting in the same wave refraction and focusing effect. However, the CMM does not compensate the lossy skull, resulting in a much lower focal energy. For the case without any complementary layer, the ultrasound through the skull directly focuses at a point approximately 3 cm to the left compared with the other cases [Fig. 4(d)]. This is because the skull has a different refractive index compared with the water and brain, and the resultant wave refraction changes the location of the focal point. The focused acoustic energy is also low because most of the acoustic waves are reflected or damped by the skull.

In conclusion, we have obtained the values of the material parameters needed for the NHCMM to compensate a lossy skull barrier. The density and sound speed of the NHCMM are the direct opposite of those of the skull, which suppress the impedance mismatch of the skull barrier. The opposite imaginary parts of the material parameters indicate the use of an active gain element which compensates for the energy loss through the skull. The ultrasonic imaging of a

brain tumor and the focusing through the complemented skull demonstrate an effective performance of the NHCMM. This NHCMM sets the foundation for noninvasive ultrasonic brain imaging and neuron disease treatments that require high frequency ultrasound.

See the [supplementary material](#) for details of the shear wave interaction with the NHCMM-skull bilayer for normal incidence, ultrasonic imaging, and HIFU therapy, in addition to methods used to experimentally realize NHCMMs through the determination of active circuit elements needed to accurately control the desired effective material parameters of the system.

This work is supported by Georgia Tech Faculty Startup Funding.

REFERENCES

- ¹J. A. Jensen, "A model for the propagation and scattering of ultrasound in tissue," *J. Acoust. Soc. Am.* **89**, 182–190 (1991).
- ²A. Fenster, D. B. Downey, and H. N. Cardinal, "Three-dimensional ultrasound imaging," *Phys. Med. Biol.* **46**, R67–R99 (2001).
- ³A. Neisius, N. B. Smith, G. Sankin, N. J. Kuntz, J. F. Madden, D. E. Fovargue, S. Mitran, M. E. Lipkin, W. N. Simmons, G. M. Preminger *et al.*, "Improving the lens design and performance of a contemporary electromagnetic shock wave lithotripter," *Proc. Natl. Acad. Sci. U. S. A.* **111**, E1167–E1175 (2014).
- ⁴J. E. Kennedy, "High-intensity focused ultrasound in the treatment of solid tumours," *Nat. Rev. Cancer* **5**, 321–327 (2005).
- ⁵A. D. Maxwell, G. Owens, H. S. Gurm, K. Ives, D. D. Myers, Jr., and Z. Xu, "Noninvasive treatment of deep venous thrombosis using pulsed ultrasound cavitation therapy (histotripsy) in a porcine model," *J. Vasc. Inter. Rad.* **22**, 369–377 (2011).
- ⁶W. J. Elias, D. Huss, T. Voss, J. Loomba, M. Khaled, E. Zadicario, R. C. Frynsinger, S. A. Sperling, S. Wylie, S. J. Monteith *et al.*, "A pilot study of focused ultrasound thalamotomy for essential tremor," *N. Engl. J. Med.* **369**, 640–648 (2013).
- ⁷M. Kinoshita, N. McDonald, F. A. Jolesz, and K. Hynynen, "Noninvasive localized delivery of Herceptin to the mouse brain by MRI-guided focused ultrasound-induced blood-brain barrier disruption," *Proc. Natl. Acad. Sci. U. S. A.* **103**, 11719–11723 (2006).
- ⁸F. J. Fry and J. E. Barger, "Acoustical properties of the human skull," *J. Acoust. Soc. Am.* **63**, 1576–1590 (1978).
- ⁹H. Chen and C. T. Chan, "Acoustic cloaking and transformation acoustics," *J. Phys. D: Appl. Phys.* **43**, 113001 (2010).
- ¹⁰S. A. Cummer, J. Christensen, and A. Alu, "Controlling sound with acoustic metamaterials," *Nat. Rev. Mater.* **1**, 16001 (2016).
- ¹¹C. Shen, J. Xu, N. X. Fang, and Y. Jing, "Anisotropic complementary acoustic metamaterial for canceling out aberrating layers," *Phys. Rev. X* **4**, 041033 (2014).
- ¹²Z. Liu, X. Zhang, Y. Mao, Y. Y. Zhu, Z. Yang, C. T. Chan, and P. Sheng, "Locally resonant sonic materials," *Science* **289**, 1734–1736 (2000).
- ¹³N. Fag, D. Xi, J. Xu, M. Ambati, W. Sritravanich, C. Sun, and X. Zhang, "Ultrasonic metamaterials with negative modulus," *Nat. Mater.* **5**, 452–456 (2006).
- ¹⁴M. Yag, G. Ma, Z. Yang, and P. Sheng, "Coupled membranes with doubly negative mass density and bulk modulus," *Phys. Rev. Lett.* **110**, 134301 (2013).
- ¹⁵T. Brnet, A. Merlin, B. Mascaró, K. Zimny, J. Leng, O. Poncelet, C. Aristégui, and O. Mondain-Monval, "Soft 3D acoustic metamaterial with negative index," *Nat. Mater.* **14**, 384–388 (2015).
- ¹⁶R. Fleury, D. Sounas, and A. Alu, "An invisible acoustic sensor based on parity-time symmetry," *Nat. Commun.* **6**, 5905 (2015).
- ¹⁷C. Shi, M. Dubois, Y. Chen, L. Cheng, H. Ramezani, Y. Wang, and X. Zhang, "Accessing the exceptional points of parity-time symmetric acoustics," *Nat. Commun.* **7**, 11110 (2016).
- ¹⁸B.-I. Popa and S. A. Cummer, "Non-reciprocal and highly nonlinear active acoustic metamaterials," *Nat. Commun.* **5**, 3398 (2014).

- ¹⁹B.-I. Popa, D. Shinde, A. Konneker, and S. A. Cummer, "Active acoustic metamaterials reconfigurable in real time," *Phys. Rev. B* **91**, 220303(R) (2015).
- ²⁰X. Zhu, H. Ramezani, C. Shi, J. Zhu, and X. Zhang, "PT-symmetric acoustics," *Phys. Rev. X* **4**, 031042 (2014).
- ²¹H. Ramezani, M. Dubois, Y. Wang, Y. R. Shen, and X. Zhang, "Directional excitation without breaking reciprocity," *New J. Phys.* **18**, 095001 (2016).
- ²²Y. Auregan and V. Pagneux, "PT-symmetric scattering in flow duct acoustics," *Phys. Rev. Lett.* **118**, 174301 (2017).
- ²³T. Liu, X. Zhu, F. Chen, S. Liang, and J. Zhu, "Unidirectional wave vector manipulation in two-dimensional space with an all passive acoustic parity-time-symmetric metamaterial crystal," *Phys. Rev. Lett.* **120**, 124502 (2018).
- ²⁴V. Fokin, M. Ambati, C. Sun, and X. Zhang, "Method for retrieving effective properties of locally resonant acoustic metamaterials," *Phys. Rev. B* **76**, 144302 (2007).
- ²⁵N. Engheta, "Pursuing near-zero response," *Science* **340**, 286–287 (2013).
- ²⁶M. Dubois, C. Shi, X. Zhu, Y. Wang, and X. Zhang, "Observation of acoustic Dirac-like cone and double zero refractive index," *Nat. Commun.* **8**, 14871 (2017).